Numerical Treatment of Nonrectangular Field-Oxide for 3-D MOSFET Simulation

MARTIN THURNER, MEMBER, IEEE, PHILIPP LINDORFER, AND SIEGFRIED SELBERHERR, SENIOR MEMBER, IEEE

Abstract—**Presently there exists only a few three-dimensional simulation programs that take into account effects at the channel edge due to nonplanar interfaces. The finite element method is mostly used for discretization to deal with those interfaces. Another approach has been successfully implemented into MINIMOS to simulate three-dimensional effects. We applied the box integration method after Forsythe for discretization. This method is excellently suitable for nonplanar interfaces. The most important nonplanar interface occurs at the transition of the gate oxide to the field oxide, which is commonly called "bird's beak." Approximating this interface with right angles leads to unrealistic results. This paper introduces the new numerical treatment in three-dimensional MOSFET simulation with nonplanar interfaces. We present the physical model used and show the numerical implementation of the basic equations. The simulations have been carried out with MINIMOS 5, our fully three-dimensional simulation program. Three-dimensional effects like threshold shift for small channel devices, channel narrowing, and the enhanced conductivity at the channel edge have been successfully modeled.**

I. Introduction

Shrinking dimensions of the single MOSFET in ULSI circuits brought up the need for suitable device models in physics and mathematics. With two-dimensional device simulators the electrical characteristics of wide-channel transistors can be described fairly well. Advanced ULSI technology, however, has led to serious problems in modeling very narrow-channel devices, and therefore, a great demand appeared for three-dimensional simulations [3], [14], [16], [22]. The three-dimensional effects in MOSFET's, like the shift of the threshold voltage, enhanced conductivity, or the large depletion region at the channel edge near to the drain caused by the finite channel width are not taken into account by two-dimensional simulations [19]. Furthermore, as the channel edge is usually defined by the "bird's beak" produced by local oxidation of silicon (LOCOS), the channel width may not be assumed to be a constant with respect to the coordinate perpendicular to the wafer surface. Therefore, it is necessary to incorporate possibilities for modeling nonplanar geometries into the program.

Unfortunately, vast amounts of CPU time and memory are needed for fully three-dimensional simulations, so very skilled and efficient algorithms have to be used. Demands on computer resources are normally kept moderate by using rectangular geometries. A new concept of treating nonplanar interfaces, while using a rectangular simulation volume has been developed. It has been implemented in MINIMOS 5, which is an integrated two- and three-dimensional device simulator for silicon MOSFET's with small signal analysis capabilities.

Section II deals with some physical and numerical aspects of three-dimensional simulations, while Section III describes the implementation of the basic equations in MINIMOS 5. Section IV reports some examples which show the capabilities of three-dimensional simulation.

Manuscript received August 3, 1989; revised February 14, 1990. This paper was recommended by Associate Editor M. Rudan.

M. Thurner is with the Campus-Based Engineering Center, Digital Equipment Corporation, A-1040 Wien, Austria.

P. Lindorfer and S. Selberherr are with the Institut für Mikroelectronik, Technische Universitat Wien, A-1040 Wien, Austria.

IEEE Log Number 9038017.

II. MINIMOS 5

2.1. Physical Model

MINIMOS 5 solves the basic semiconductor equations (2.1)–(2.3) in their stationary form which have been completely presented for the first time by VanRoosbroeck [24]:

$$\text{div grad } \psi = \frac{q}{\epsilon} \cdot (n - p - C) \tag{2.1}$$

$$\text{div } J_n = q \cdot R \tag{2.2}$$

$$\text{div } J_p = -q \cdot R. \tag{2.3}$$

During the past ten years MINIMOS has been improved continuously. Enhancements and extensions have been achieved on one hand by improved models for physical parameters and on the other hand by adding further steps in an hierarchical order to the iterative solving process. The solution of each step is based on the previous one and incorporates additional effects which have been neglected before. A major improvement has been achieved by including a hot electron model [12], [13] which takes into account hot carrier effects. This model uses slightly different current relations (2.4) and (2.5) with electronic voltages describing the heating of electrons and holes. A new model for the carrier mobilities has been included to guarantee a consistent set of equations:

$$J_n = q \cdot \mu_n \cdot n \cdot \left(-\text{grad } \psi + \frac{1}{n} \cdot \text{grad } (U_{t_n} \cdot n) \right) \tag{2.4}$$

0278-0070/90/1100-1189$01.00 © 1990 IEEE

$$J_p = q \cdot \mu_p \cdot p \cdot \left(-\text{grad}\ \psi - \frac{1}{p} \cdot \text{grad}\ (U_{t_p} \cdot p) \right) \tag{2.5}$$

$$\mu_n^{\text{LISF}} = \frac{2 \cdot \mu_n^{\text{LIS}}}{1 + \sqrt{1 + \left(\dfrac{2 \cdot \mu_n^{\text{LIS}} \cdot F_n}{v_n^{\text{sat}}} \right)^2}}$$

$$\mu_p^{\text{LISF}} = \frac{\mu_p^{\text{LIS}}}{1 + \left(\dfrac{\mu_p^{\text{LIS}} \cdot F_p}{v_p^{\text{sat}}} \right)} \tag{2.6}$$

$$F_n = \left| \text{grad}\ \psi - \frac{1}{n}\ \text{grad}\ (n \cdot Ut_n) \right|$$
$$F_p = \left| \text{grad}\ \psi + \frac{1}{p}\ \text{grad}\ (p \cdot Ut_p) \right| \tag{2.7}$$

$$Ut_{n,p} = Ut_0 + \frac{2}{3} \cdot \tau_{n,p}^{\epsilon} \cdot (v_{n,p}^{\text{sat}})^2 \cdot \left(\frac{1}{\mu_{n,p}^{\text{LISF}}} - \frac{1}{\mu_{n,p}^{\text{LIS}}} \right). \tag{2.8}$$

$\mu_{n,p}^{\text{LIS}}$ denotes the mobility influenced by lattice-, ionized impurities-, and surface-scattering (cf. [2], [18]). The driving forces $F_{n,p}$ are given by (2.7). In (2.8) the model of the electronic voltages is given, where $\tau_{n,p}^{\epsilon}$ denotes the energy relaxation time of electrons and holes. A discussion of this formulation can be found in [11].

The most recent milestone in the evolution of MINIMOS is the extension from two to three space dimensions [21]. Following the approach of two-dimensional MINIMOS a similar hierarchical solving process is applied in the three-dimensional case. The two-dimensional simulation starts with a simple one-carrier model, takes into account avalanche generation for both carrier types—if requested—and stops with the solution of the hot electron model. The three-dimensional simulation takes a two-dimensional solution as an initial guess and solves as a first step only the Poisson equation (2.1) in three dimensions whereas the carrier densities of electrons and holes are only extended into the third dimension using the quasi-Fermi levels:

$$n_{x,y,z} = n_{x,y,z|w/2} \cdot \exp\left(-\frac{1}{U_t} \cdot (\psi_{x,y,z|w/2} - \psi_{x,y,z}) \right) \tag{2.9}$$

$$p_{x,y,z} = p_{x,y,z|w/2} \cdot \exp\left(+\frac{1}{U_t} \cdot (\psi_{x,y,z|w/2} - \psi_{x,y,z}) \right). \tag{2.10}$$

The index $w/2$ denotes the middle of the channel width. The underlying assumptions for this first step are:

- negligible current flow in the direction of the channel width which is plausible in the absence of contacts which would cause great potential differences in this direction:
$$J_{n_z} = J_{p_z} = 0. \tag{2.11}$$
- Boltzmann statistics are assumed to be valid in channel width direction which means constant quasi-Fermi levels:
$$\frac{\partial \varphi_n}{\partial z} = \frac{\partial \varphi_p}{\partial z} = 0. \tag{2.12}$$

This model allows a relatively "simple" and "fast" solution in terms of three-dimensional calculations and gives sufficiently accurate solutions especially in the subthreshold region. Like the two-dimensional simulation a fully automatic grid adaption is performed.

The second step of the three-dimensional simulation solves the Poisson equation as well as the two continuity equations fully three-dimensionally, including avalanche generation and carrier heating, if requested. This model gives accurate results also under high bias conditions. The second step is very CPU-time and memory consuming, because of Gauß elimination which is used for solving the continuity equations. At present strong efforts are made to speedup the solution of these equations by means of new algorithms.

Capabilities of future versions of MINIMOS will be transient simulations and the simulation of GaAs-MESFET's. Therefore, models for carrier transport in GaAs and Schottky boundary conditions as well as algorithms for time dependent simulations are now under investigation.

2.2. *Numerical Aspects*

The discretization in MINIMOS is based on a finite difference grid. This method is superior to other discretization schemes, especially when using rectangular bounded simulation domains. In this approach meshlines and boundaries coincide and one can obtain the discrete boundary conditions easily [17]. In the first version of three-dimensional MINIMOS the finite difference discretization has been implemented since only rectangular interfaces have been used. It turned out, however, that it is necessary to consider nonplanarities, especially in the direction of the channel width to obtain realistic results for narrow channel devices. To maintain the finite difference grid, a special technique is applied to allow arbitrarily shaped interfaces in the rectangular grid. This technique uses the box integration method after Forsythe [6] for discretization to obtain implicit boundary conditions which will not destroy the structure of the matrix of the linear system—compared to the finite element method, which is mostly used for nonplanar geometries. A detailed description will be given in Section III. One main advantage of this method is that the matrices one obtains are very sparse and structured, i.e., that one has only five nonzero diagonals in the matrix for the two-dimensional and seven for the three-dimensional case, respectively. This implies that one can use very efficient and specialized solvers—also specialized for different computer architectures—for solv-

ing the linear system which is of major importance in case of three-dimensional simulations where the typical rank of the matrix goes from 50 000 to 100 000. A typical example with 60 000 gridpoints is solved in 3.5 CPU hours on a VAX 6240. The interested reader is referred to, e.g., [7], [8], [10].

At this point a few comments should be made on the calculation of the terminal currents. Due to the nonrectangular field oxide the channel width is not constant over the channel depth. Therefore, the problem arises on how to define the proper channel width which has to be used to calculate the terminal currents from the two-dimensional simulation. The oxide reduces gradually the channel width which is given by the mask specifications. This situation is shown in Fig. 1. To tackle this problem we introduce an effective channel width w_{eff} for the two-dimensional current calculation instead of the given mask width. The effective channel width is calculated by

$$w_{\text{eff}} = w - \frac{1}{D_{\text{ch}}} \int_0^w fox(z)\big|_{l/2}\, dz \qquad (2.13)$$

where w is the width specified by the mask, D_{ch} denotes the channel depth at the channel edge (Fig. 1 vertical dashed line crossing the interface line), $l/2$ denotes half of the channel length, and $fox(z)$ is the function which describes the geometry of the channel in width direction.

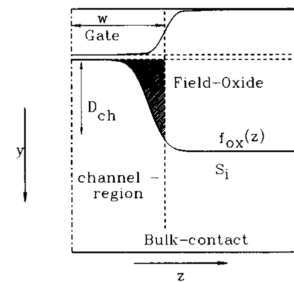

Fig. 1. Cross-sectional view of a MOSFET channel in width direction.

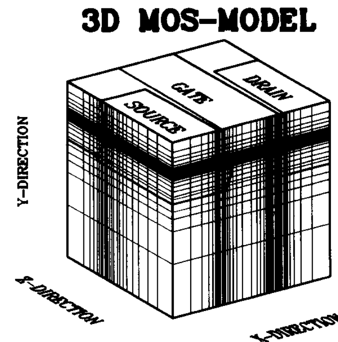

Fig. 2. Perspective view of the three-dimensional MOSFET structure with discretization grid.

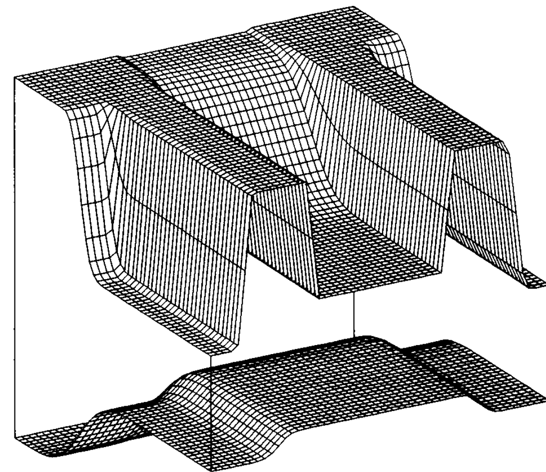

Fig. 3. Oxide body of a MOSFET structure (the oxide is between the upper and lower plane).

2.3. Device Structures

Using a finite difference scheme for discretization usually leads to a rectangular bounded simulation volume. This simulation volume consists of different regions separated either by physical or artificial boundaries. There are essentially three different regions in a MOSFET: the contacts, the oxide, and the semiconductor. A physical boundary, for example, is the interface between the oxide and the semiconductor whereas artificial boundaries are introduced to separate the single device in a chip for simulation. To obtain realistic results, one has to consider the nonplanar shape of the interfaces especially in the direction of the channel width. Fig. 2 shows such a simulation cube with the grid and the nonplanar interfaces. It should be mentioned that Fig. 2 shows a cube with geometry data and a grid actually used by MINIMOS. Nonplanarities are treated in the way that the oxide volume ("oxide body") of a MOSFET, which exists between the contacts and the semiconductor, is described by two interfaces: the interface between metallic contacts and the oxide and the interface between the oxide and the semiconductor, respectively.

One of the most general device structures we are able to simulate, is plotted in Fig. 3. One can see the source contact on the left hand, the gate strip in the middle, and the drain contact on the right. The thin gate oxide in the middle spreads up to the field oxide in the direction of the channel width, where one can see the characteristic bird's beak. Source and drain contacts are recessed into silicon due to a reoxidation. For the sake of visibility the two interfaces are expanded.

It has to be mentioned that geometry data can easily be provided by the user via the input deck. About 25 parameters can be used in the present version specifying distances and transition lengths to define the shape of the contacts and the semiconductor surface (most of the 25

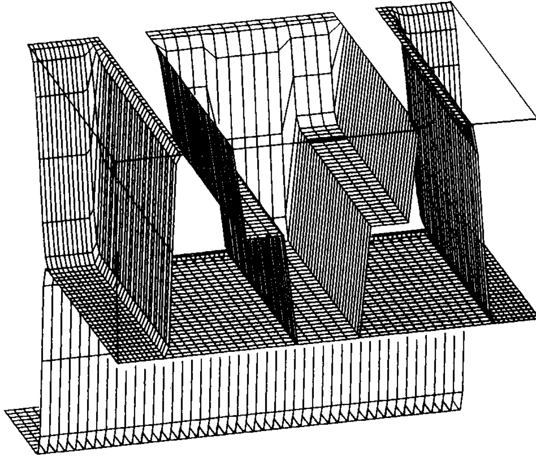

Fig. 4. Device structure of a T-gate MESFET.

parameters have default values if not specified). For use of geometry data obtained from a process simulator, a standardized interface for these data will be implemented in a future version. Fig. 4 shows another example which can be defined easily by the user. It shows a T-gate structure commonly used in todays MESFET's for controlling ion implantation between the contacts. One can clearly see the T-like shape of the gate contact on the planar semiconductor surface. Of course, the term "oxide body" cannot be used in this case, but the approach for treating these nonplanarities remains the same.

III. The Discretization of the Basic Equations

The physical model for the simulation has been characterized in the previous section. The basic semiconductor equations cannot be solved explicitly in general. Therefore, the solution must be calculated by means of numerical approaches. Dividing the domain—the simulation region—into a finite number of subdomains, in which the solution can be approximated easily [5], [15], we use the classical finite difference grid for the three dimensions (x, y, z). The coupled nonlinear difference equations—the basic semiconductor equations—are solved essentially with Gummel's iterative method [9]. Finally the set of linearized equations with the huge number of unknowns arising from the discretization scheme are solved with iterative methods. For detailed information on numerical aspects for solving large systems of linear equations, the interested reader is referred to, e.g., [7], [8], [25]. For discretization we apply the box integration method after Forsythe [6] to deal with the boundary conditions of the nonrectangular interfaces. The discretization of the Dirichlet boundary conditions for the contact regions and of the Neumann boundary conditions for the artificial boundaries is straightforward and can be found in [17].

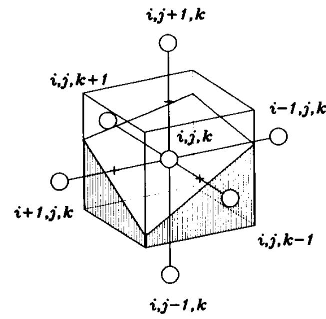

Fig. 5. Perspective view of a discretization point at the interface, e.g., oxide-semiconductor interface (hatched part denotes the volume in the semiconductor).

3.1 Poisson's Equation

The boundary condition for Poisson's equation at the interface is given by

$$\epsilon_{\text{ins}} \frac{\partial \psi}{\partial \vec{n}}\bigg|_{\text{ins}} = \epsilon_{\text{sem}} \frac{\partial \psi}{\partial \vec{n}}\bigg|_{\text{sem}} - \sigma_{\text{int}} \tag{3.1}$$

where ϵ denotes the permittivity; the indexes ins, sem, int denote the insulator, semiconductor, and the interfaces, and σ_{int} denotes the charge at the interface. We shall discuss the discretization method for the nonrectangular interface boundary conditions (3.1) in detail, since by now nonplanar interfaces have been implemented only in device simulation programs using finite elements. A point close to the interface is shown in Fig. 5. The surrounding finite integration volume is divided into two parts; one below the interface (hatched in this picture), representing the semiconductor region and one above the interface, representing the oxide region. In this picture we can also see the discretization grid and the neighboring points. Integrating (3.1) over the interface element F_i we obtain

$$\int_{F_i} \epsilon_{\text{sem}} \frac{\partial \psi}{\partial \vec{n}}\, do = \int_{F_i} \epsilon_{\text{sem}} \operatorname{grad} \psi|_{\text{sem}} \cdot \vec{n}\, do = \int_{F_i} \epsilon_{\text{ins}} \operatorname{grad} \psi|_{\text{ins}} \cdot \vec{n}\, do + \int_{F_i} \sigma_{\text{int}}\, do. \tag{3.2}$$

For each point at the interface we can write the Poisson equation in the semiconductor and the Laplace equation in the insulating material. Both equations are integrated over the respective volume (V_{sem}, V_{ins}).

In the semiconductor region we obtain

$$\int_{V_{\text{sem}}} \operatorname{div}(\epsilon_{\text{sem}} \cdot \operatorname{grad} \psi)\, dv = \int_{V_{\text{sem}}} \rho\, dv. \tag{3.3}$$

In the insulating region we obtain

$$\int_{V_{\text{ins}}} \operatorname{div}(\epsilon_{\text{ins}} \cdot \operatorname{grad} \psi)\, dv = 0. \tag{3.4}$$

Using the law of Gauß and splitting the surface integral into its components (remembering the discretization grid) we can rewrite (3.3) and (3.4):

$$\oint_{O_{sem}} (\epsilon_{sem} \cdot \text{grad}\, \psi)\, \vec{do} = \int_{F1_{sem}} (\epsilon_{sem} \cdot \text{grad}\, \psi)\, \vec{do} + \int_{F2_{sem}} (\epsilon_{sem} \cdot \text{grad}\, \psi)\, \vec{do} + \int_{F3_{sem}} (\epsilon_{sem} \cdot \text{grad}\, \psi)\, \vec{do} + \int_{F4_{sem}} (\epsilon_{sem} \cdot \text{grad}\, \psi)\, \vec{do} + \int_{F5_{sem}} (\epsilon_{sem} \cdot \text{grad}\, \psi)\, \vec{do} + \int_{F6_{sem}} (\epsilon_{sem} \cdot \text{grad}\, \psi)\, \vec{do} + \int_{F_i} (\epsilon_{sem} \cdot \text{grad}\, \psi)\, \vec{do} = \int_{V_{sem}} \rho\, dv \quad (3.5)$$

$$\oint_{O_{ins}} (\epsilon_{ins} \cdot \text{grad}\, \psi)\, \vec{do} = \int_{F1_{ins}} (\epsilon_{ins} \cdot \text{grad}\, \psi)\, \vec{do} + \int_{F2_{ins}} (\epsilon_{ins} \cdot \text{grad}\, \psi)\, \vec{do} + \int_{F3_{ins}} (\epsilon_{ins} \cdot \text{grad}\, \psi)\, \vec{do} + \int_{F4_{ins}} (\epsilon_{ins} \cdot \text{grad}\, \psi)\, \vec{do} + \int_{F5_{ins}} (\epsilon_{ins} \cdot \text{grad}\, \psi)\, \vec{do} + \int_{F6_{ins}} (\epsilon_{ins} \cdot \text{grad}\, \psi)\, \vec{do} + \int_{F_i} (\epsilon_{ins} \cdot \text{grad}\, \psi)\, \vec{do} = 0. \quad (3.6)$$

The integration areas F denote the boundaries of the finite integration volume and the indexes sem and ins denote the parts in the semiconductor and the insulator, respectively. The indexes $(1 \cdots 6)$ of the integration areas define the position and the orientation in the following way: F_1 denotes the area perpendicular to the z-axis in the middle of the grid lines (k) and $(k - 1)$, F_2 denotes the area perpendicular to the y-axis in the middle of the grid lines (j) and $(j - 1)$, F_3 denotes the area perpendicular to the x-axis in the middle of the grid lines (i) and $(i - 1)$, F_4 denotes the area perpendicular to the x-axis in the middle of the grid lines (i) and $(i + 1)$, F_5 denotes the area perpendicular to the y-axis in the middle of the grid lines (j) and $(j + 1)$, and F_6 denotes the area perpendicular to the z-axis in the middle of the grid lines (k) and $(k + 1)$. The integration area F_i is the interface element.

Using (3.5) and (3.6) we can now substitute the gradients of ψ perpendicular to the interface in (3.2) and thus we obtain (3.7).

$$\int_{V_{sem}} \rho\, dv + \int_{F_i} \sigma_{int}\, do = \epsilon_{sem} \cdot \left(\int_{F1_{sem}} \text{grad}\, \psi\, \vec{do} + \int_{F2_{sem}} \text{grad}\, \psi\, \vec{do} + \int_{F3_{sem}} \text{grad}\, \psi\, \vec{do} + \int_{F4_{sem}} \text{grad}\, \psi\, \vec{do} + \int_{F5_{sem}} \text{grad}\, \psi\, \vec{do} + \int_{F6_{sem}} \text{grad}\, \psi\, \vec{do} \right) + \epsilon_{ins} \cdot \left(\int_{F1_{ins}} \text{grad}\, \psi\, \vec{do} + \int_{F2_{ins}} \text{grad}\, \psi\, \vec{do} + \int_{F3_{ins}} \text{grad}\, \psi\, \vec{do} + \int_{F4_{ins}} \text{grad}\, \psi\, \vec{do} + \int_{F5_{ins}} \text{grad}\, \psi\, \vec{do} + \int_{F6_{ins}} \text{grad}\, \psi\, \vec{do} \right). \quad (3.7)$$

The discretization of the terms in (3.7) is quite simple, suitable approximations can be found in, e.g., [17], [21], and we can write the discretized equation in a more formal way by

$$\begin{aligned} &\psi_{i,j,k-1} \cdot (A_{sem} \cdot \epsilon_{sem} + A_{ins} \cdot \epsilon_{ins}) \cdot \frac{1}{n_{k-1}} \\ &+ \psi_{i,j-1,k} \cdot (B_{sem} \cdot \epsilon_{sem} + B_{ins} \cdot \epsilon_{ins}) \cdot \frac{1}{m_{j-1}} \\ &+ \psi_{i-1,j,k} \cdot (C_{sem} \cdot \epsilon_{sem} + C_{ins} \cdot \epsilon_{ins}) \cdot \frac{1}{l_{i-1}} \\ &- \psi_{i,j,k} \cdot (G_{sem} \cdot \epsilon_{sem} + G_{ins} \cdot \epsilon_{ins}) \\ &+ \psi_{i+1,j,k} \cdot (D_{sem} \cdot \epsilon_{sem} + D_{ins} \cdot \epsilon_{ins}) \cdot \frac{1}{l_i} \\ &+ \psi_{i,j+1,k} \cdot (E_{sem} \cdot \epsilon_{sem} + E_{ins} \cdot \epsilon_{ins}) \cdot \frac{1}{m_j} \\ &+ \psi_{i,j,k+1} \cdot (F_{sem} \cdot \epsilon_{sem} + F_{ins} \cdot \epsilon_{ins}) \cdot \frac{1}{n_k} \\ &= (\rho_{i,j,k} \cdot V_{sem} + \sigma_{i,j,k} \cdot A_{int}). \end{aligned} \quad (3.8)$$

A, B, C, D, E, F correspond to the areas $F_1, F_2, F_3, F_4, F_5, F_6$, and the coefficient G is the sum of the coefficients (A/n_{k-1}), (B/m_{j-1}), (C/l_{i-1}), (D/l_i), (E/m_j), (F/n_k), where l, m, n are the distances to the neighboring points in x, y, and z direction, respectively (see Fig. 5). The indexes sem and ins denote the sections of the areas in the semiconductor and the insulator, respectively. ϵ is the permittivity, σ is the interface charge, ρ is the space charge, and A_{int} is the interface area.

3.2 Continuity Equation

The discretization of the continuity equation at points which are located totally within the semiconductor region can be found in various publications [17]. We shall present the numerical treatment of the boundary conditions for the continuity equation at nonrectangular interfaces by means of the box integration method. The interface conditions are

$$\vec{J}_n \cdot \vec{n} = -q \cdot R^{\text{surf}}$$
$$\vec{J}_p \cdot \vec{n} = +q \cdot R^{\text{surf}}. \tag{3.9}$$

For the electrons we integrate the boundary condition (3.9) over the interface element F_i and obtain

$$\int_{F_i} \vec{J}_n \cdot \vec{do} = \int_{F_i} \vec{J}_n \cdot \vec{n}\, do = \int_{F_i} -q \cdot R^{\text{surf}}\, do. \tag{3.10}$$

Furthermore, the continuity equation (3.2) must hold in the semiconductor region at the interface. So we can evaluate the volume integral:

$$\int_V \text{div}\, \vec{J}_n\, dv = \int_{V_{\text{sem}}} \text{div}\, \vec{J}_n\, dv = \int_{V_{\text{sem}}} -q \cdot R\, dv. \tag{3.11}$$

Using Gauß's law and remembering the discretization grid we can write:

$$\begin{aligned}\int_{V_{\text{sem}}} \text{div}\, \vec{J}_n\, dv &= \oint_{O_{\text{sem}}} \vec{J}_n\, \vec{do} \\ &= \int_{F1_{\text{sem}}} \vec{J}_n\, \vec{do} + \int_{F2_{\text{sem}}} \vec{J}_n\, \vec{do} + \int_{F3_{\text{sem}}} \vec{J}_n\, \vec{do} \\ &\quad + \int_{F4_{\text{sem}}} \vec{J}_n\, \vec{do} + \int_{F5_{\text{sem}}} \vec{J}_n\, \vec{do} + \int_{F6_{\text{sem}}} \vec{J}_n\, \vec{do} \\ &\quad + \int_{F_i} \vec{J}_n\, \vec{do} \\ &= \int_{V_{\text{sem}}} -q \cdot R\, dv. \end{aligned} \tag{3.12}$$

The integration areas F and their indexes have been described in the previous section. The discretization of the currents penetrating the areas F_1 to F_6 can be found in, e.g., [17], [21]. Thus we can substitute (3.12) into (3.10) and obtain

$$\begin{aligned}&\int_{F1_{\text{sem}}} \vec{J}_n\, \vec{do} + \int_{F2_{\text{sem}}} \vec{J}_n\, \vec{do} + \int_{F3_{\text{sem}}} \vec{J}_n\, \vec{do} \\ &\quad + \int_{F4_{\text{sem}}} \vec{J}_n\, \vec{do} + \int_{F5_{\text{sem}}} \vec{J}_n\, \vec{do} + \int_{F6_{\text{sem}}} \vec{J}_n\, \vec{do} \\ &\quad = \int_{V_{\text{sem}}} -q \cdot R\, dv + \int_{F_i} q \cdot R^{\text{surf}}\, do. \end{aligned} \tag{3.13}$$

Using a suitable discretization for the current densities we can write the discretized boundary condition at the semiconductor oxide interface by

$$\begin{aligned}&n(x_i, y_j, z_{k+1}) \cdot \frac{\mu_n(x_i, y_j, z1)}{\xi_{z1}} \cdot B(\eta_{z1} \cdot \xi_{z1}) \cdot A_{\text{sem}} \\ &\quad + n(x_i, y_j, z_{k-1}) \cdot \frac{\mu_n(x_i, y_j, z0)}{\xi_{z0}} \cdot B(\eta_{z0} \cdot \xi_{z0}) \\ &\quad \cdot B_{\text{sem}} + n(x_{i+1}, y_j, z_k) \cdot \frac{\mu_n(x1, y_j, z_k)}{\xi_{x1}} \\ &\quad \cdot B(\eta_{x1} \cdot \xi_{x1}) \cdot C_{\text{sem}} + n(x_{i-1}, y_j, z_k) \\ &\quad \cdot \frac{\mu_n(x0, y_j, z_k)}{\xi_{x0}} \cdot B(\eta_{x0} \cdot \xi_{x0}) \cdot D_{\text{sem}} \\ &\quad + n(x_i, y_{j+1}, z_k) \cdot \frac{\mu_n(x_i, y1, z_k)}{\xi_{y1}} \cdot B(\eta_{y1} \cdot \xi_{y1}) \\ &\quad \cdot E_{\text{sem}} + n(x_i, y_{j-1}, z_k) \cdot \frac{\mu_n(x_i, y0, z_k)}{\xi_{y0}} \\ &\quad \cdot B(\eta_{y0} \cdot \xi_{y0}) \cdot F_{\text{sem}} - n(x_i, y_j, z_k) \cdot \\ &\quad \cdot \left(\frac{\mu_n(x_i, y_j, z1)}{\xi_{z1}} \cdot B(-\eta_{z1} \cdot \xi_{z1}) \cdot A_{\text{sem}} \right. \\ &\quad + \frac{\mu_n(x_i, y_j, z0)}{\xi_{z0}} \cdot B(-\eta_{z0} \cdot \xi_{z0}) \cdot B_{\text{sem}} \\ &\quad + \frac{\mu_n(x1, y_j, z_k)}{\xi_{x1}} \cdot B(-\eta_{x1} \cdot \xi_{x1}) \cdot C_{\text{sem}} \\ &\quad + \frac{\mu_n(x0, y_j, z_k)}{\xi_{x0}} \cdot B(-\eta_{x0} \cdot \xi_{x0}) \cdot D_{\text{sem}} \\ &\quad + \frac{\mu_n(x_i, y1, z_k)}{\xi_{y1}} \cdot B(-\eta_{y1} \cdot \xi_{y1}) \cdot E_{\text{sem}} \\ &\quad \left. + \frac{\mu_n(x_i, y0, z_k)}{\xi_{y0}} \cdot B(-\eta_{y0} \cdot \xi_{y0}) \cdot F_{\text{sem}} \right) \\ &\quad = -R(x_i, y_j, z_k) \cdot V_{\text{sem}} + r^{\text{SURF}}(x_i, y_j, z_k) \cdot A_{\text{int}}. \end{aligned} \tag{3.14}$$

V_{sem} is the part of the integration volume in the semiconductor, R^{SURF} denotes the surface recombination rate and A_{int} is the interface element. The coefficients ξ_{x0}, ξ_{x1}, ξ_{y0}, ξ_{y1}, ξ_{z0}, ξ_{z1}, and η_{x0}, η_{x1}, η_{y0}, η_{y1}, η_{z0}, η_{z1} include the dependence on the potential ψ and the electronic voltage Ut_n of the carriers [21]. The general expressions for ξ and η are

$$\xi = \frac{\ln\left(\frac{Ut^+_{n,p}}{Ut^0_{n,p}}\right)}{(\Delta Ut_{n,p})/h}$$

$$\eta = -\frac{\Delta\psi - \Delta Ut_{n,p}}{h} \tag{3.15}$$

where $Ut^0_{n,p}$ and $Ut^+_{n,p}$ denote the potential at the point under consideration and at the neighboring point, respectively; h is the distance between the two points. A fully analogous expression can be found for the continuity equation of the holes.

At interfaces without any recombination the equation $\vec{J}_n \cdot \vec{n} = 0$ must hold. In this special case the driving forces (2.7) have to be set to zero:

$$\vec{F}_n\big|_{int} = 0. \tag{3.16}$$

Not being aware of this interface condition we might obtain unrealistic mobilities at the interface. This condition is straightforward to include into the discretization.

IV. Some Results

For demonstrating the influence of nonplanarities in channel width direction on the device characteristic we have selected two devices which differ only in the channel width. The channel length equals 1.2 μm; the channel width specified by mask for transistor 1 is 1.0 μm whereas the width of transistor 2 is 3.0 μm. The geometry of the examples is shown in Fig. 1. Besides the field-oxide for channel stopping we applied a field-implantation to reduce the parasitic currents at the channel edge. The gate oxide is 0.015 μm and the field-oxide thickness is 0.6 μm. The doping concentration on source and drain is in the order of $1.5 \cdot 10^{20}$. The devices of our examples are biased with U_{DS} = 3.0 V, U_{GS} = 1.0 V, and U_{SB} = 0. V.

Figs. 6(a) and 7(a) show the potential distribution of both transistor 1 and transistor 2. The distribution is shown in a depth of 0.002 μm under the silicon surface. In the pictures the source contact is on the left side, whereas the drain contact is on the right. We can clearly see the higher potential on the right. Between source and drain the potential distribution in the channel is shown, extending from the middle of the device to the field oxide (see Fig. 1). The change of the potential distribution in width direction (z-direction) indicates clearly the channel edge. The carrier concentrations are illustrated in Figs. 6(b) and 7(b), where one can realize an enlarged depletion region at the channel edge near drain. For transistor 1 we

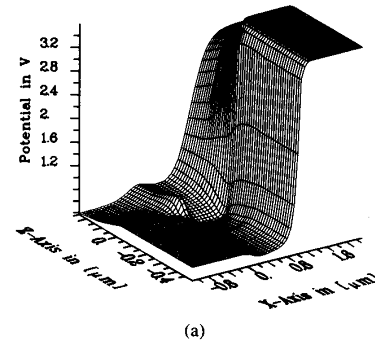

(a)

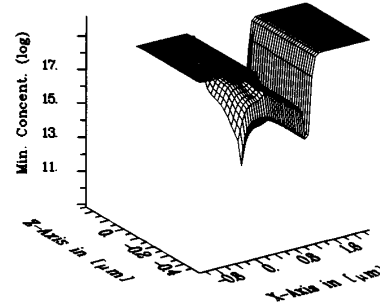

(b)

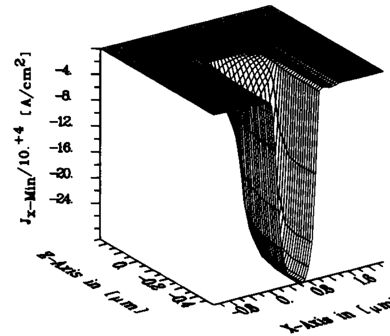

(c)

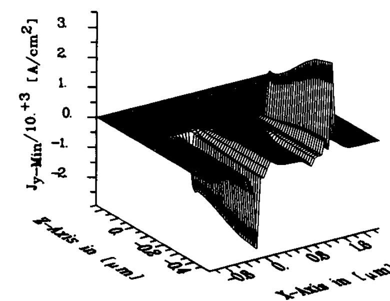

(d)

Fig. 6. (a) Potential distribution of transistor 1 at U_{GS} = 1.0 V, U_{DS} = 3.0 V, U_{SB} = 0.0 V. (b) Minority carrier distribution of transistor 1 at U_{GS} = 1.0 V, U_{DS} = 3.0 V, U_{SB} = 0.0 V. (c) Current density component in x- direction of the minority carriers of transistor 1 at U_{GS} = 1.0 V, U_{DS} = 3.0 V, U_{SB} = 0.0 V. (d) Current density component in y-direction of the minority carriers of transistor 1 at U_{GS} = 1.0 V, U_{DS} = 3.0 V, U_{SB} = 0.0 V.

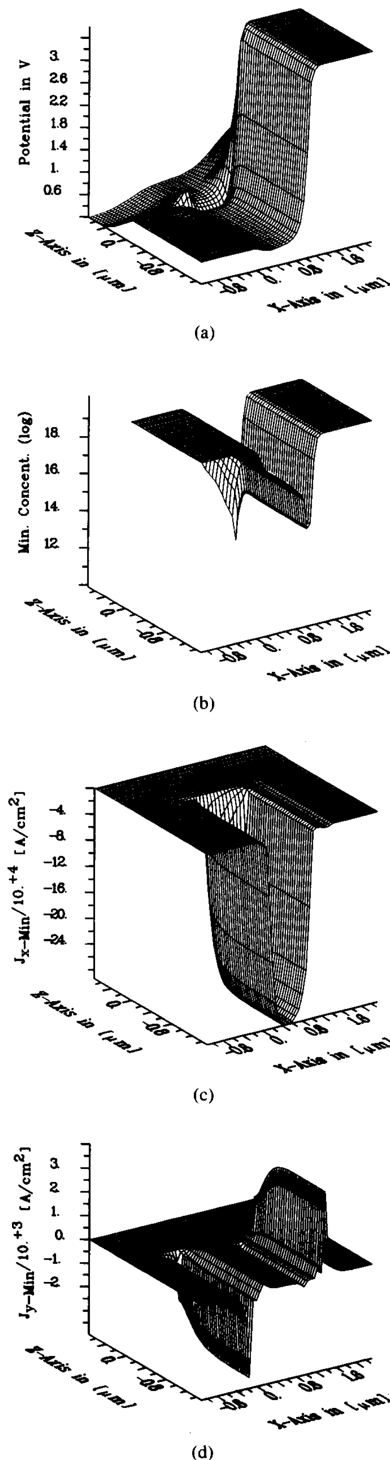

Fig. 7. (a) Potential distribution of transistor 2 at $U_{GS} = 1.0$ V, $U_{DS} = 3.0$ V, $U_{SB} = 0.0$ V. (b) Minority carrier distribution of transistor 2 at $U_{GS} = 1.0$ V, $U_{DS} = 3.0$ V, $U_{SB} = 0.0$ V. (c) Current density component in x- direction of the minority carriers of transistor 2 at $U_{GS} = 1.0$ V, $U_{DS} = 3.0$ V, $U_{SB} = 0.0$ V. (d) Current density component in y- direction of the minority carriers of transistor 2 at $U_{GS} = 1.0$ V, $U_{DS} = 3.0$ V, $U_{SB} = 0.0$ V.

can observe that the influence of the channel edge extends much more into the channel compared to transistor 2. The magnitude of this effect is the same in both devices, but the influence on the overall characteristic is much higher for the narrow channel device (1.0 μm). The same behavior can be seen with the x- and y-components of the minority current densities, as shown in Figs. 6(c), (d) and 7(c), (d). Detailed investigation on the behavior of the device characteristics due to differently shaped oxide-bodies can be found (e.g., [1], [3], [4], [23]).

V. Conclusion

We have shown that the box integration method is excellently practicable for discretization even for devices with nonplanar interfaces. Due to this method the highly optimized solver used in the simulation programs for rectangular interfaces (structured sparse matrices) are kept. The method described in this paper helps to reduce the CPU-time and memory requirements to an amount that three-dimensional simulations are now applicable for industrial use with present computer systems. Continuous improvements of both computer systems and mathematical algorithms will make future three-dimensional simulations as practicable as two-dimensional simulations are now.

References

[1] L. A. Akers, "Characterization of the inverse narrow width effect," *IEEE Trans. Electron Devices*, vol. ED-34, pp. 2476-2484, 1987.

[2] N. D. Arora and S. G. Gildenblad, "A semi-empirical model of the MOSFET inversion layer mobility for low temperature operation," *IEEE Trans. Electron Devices*, vol. ED-34, pp. 89-93, 1987.

[3] P. Ciampolini, A. Gnudi, R. Guerrieri, M. Rudan, and G. Baccarani," 3D simulation of a narrow-width MOSFET," in *ESSDERC Proc.*, 1987, pp. 413-416.

[4] J. L. Coppee, E. Figueras, B. Goffin, D. Gloesener, and F. Van De Wiele, "Narrow channel effect on n- and p-channel devices fabricated with the SILO and BOX isolation techniques," in *ESSDERC Proc.*, 1988, pp. 749-752.

[5] A. DeMari, "An accurate numerical steady-state one-dimensional solution of the P-N junction," *Solid-State Electron.*, vol. 11, pp. 33-58, 1968.

[6] G. E. Forsythe and W. R. Wasaw, *Finite Difference Methods for Partial Differential Equations*. New York: Wiley, 1960.

[7] G. H. Golub and R. S. Varga, "Chebyshev semi-iterative methods, successive overrelaxation methods, and second order Richardson iterative methods," *Num. Math.*, vol. 3, pp. 147-168, 1961.

[8] R. G. Grimes, D. R. Kincaid, and D. M. Young, "ITPACK 2A - A FORTRAN implementation of adaptive accelerated iterative methods for solving large sparse linear systems," Rep. CNA-164, Center for Numerical Analysis, Univ. of Texas at Austin, 1979.

[9] H. K. Gummel," A self-consistent iterative scheme for one-dimensional steady state transistor calculations," *IEEE Trans. Electron Devices*, ED-11, pp. 455-465, 1964.

[10] L. A. Hageman, Franklin T. Luk, and David M. Young, "On the equivalence of certain iterative acceleration methods," *SIAM J. Numer. Anal.*, vol. 17, no. 6, pp. 852-873, Dec. 1980.

[11] W. Hänsch, M. Miura-Mattausch, "A new current relation for hot electron transport," in *Proc. NASECODE IV Conf.*, 1985, pp. 311-314.

[12] P. Markowich, C. Ringhofer, and C. Schmeiser, *Semiconductor Equations*. New York: Springer-Verlag, 1989.

[13] W. Hänsch and S. Selberherr, "MINIMOS 3: A MOSFET simulator that includes energy balance," *IEEE Trans. Electron Devices*, vol. ED-34, pp. 1074-1078, 1987.

[14] A. Husain and S. G. Chamberlain, "3D simulation of VLSI MOSFET's: The 3D simulation program WATMOS," *IEEE Trans. Solid-State Circuits*, vol. SC-17, pp. 261-268, 1982.

[15] P. A. Markowich, *The Stationary Semiconductor Device Equations.* New York: Springer, 1986.
[16] S. Onga, N. Shigyo, M. Yoshimi, and K. Taniguchi, "Analysis of submicron MOS device characteristics using a composite full three-dimensional process/device simulation system," in *Proc. Symp. on VLSI Technology*, 1986, pp. 15-16.
[17] S. Selberherr, *Analysis and Simulation of Semiconductor Devices.* New York: Springer, 1984.
[18] —, "Low temperature MOS device modeling," in *Proc. Symp. Electronic Society on Low Temperature Electronics*, 1987.
[19] S. M. Sze, *Physics of Semiconductor Devices.* New York: Wiley, 1981.
[20] —, *VLSI Technology.* New York: McGraw-Hill, 1983.
[21] M. Thurner, "Dreidimensionale modellierung von MOS transistoren," Ph.D. dissertation, Technical Univ. Vienna, Wien, 1988.
[22] M. Thurner and S. Selberherr, "Comparison of long- and short-channel MOSFET's carried out by 3D-MINIMOS," in *ESSDERC Proc.*, 1987, pp. 409-412.
[23] —, "3D MOSFET device effects due to field oxide," in *ESSDERC Proc.*, 1988, pp. 245-248.
[24] W. V. Van Roosbroeck, "Theory of flow of electrons and holes in germanium and other semiconductors, *Bell Syst. Tech. J.*, vol. 29, pp. 560-607, 1950.
[25] R. S. Varga, *Matrix Iterative Analysis.* Englewood Cliffs, NJ: Prentice-Hall, 1962.

Martin Thurner (S'86-M'89) for a photograph and biography please see page 867 of the August 1990 issue of this TRANSACTIONS.

*

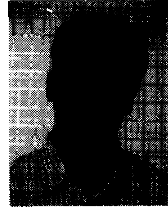

Philipp Lindorfer received the Diplomingenieur degree in communication engineering from the Technical University of Vienna in 1987. He is currently working towards the Ph.D. degree at the Institute for Microelectronics.

His interests include models for III-V Compound semiconductors in multidimensional device simulation.

*

Siegfried Selberherr (M'79-SM'84) for a photograph and biography please see page 867 of the August 1990 issue of this TRANSACTIONS.